Pergamon

Int. J. Heat Mass Transfer. Vol. 39, No. 1, pp. 27–37, 1996
Elsevier Science Ltd
Printed in Great Britain

0017–9310(95)00104–2

Effects of Dean vortex pairs on surface heat transfer in curved channel flow

P. M. LIGRANI and S. CHOI
Department of Mechanical Engineering, University of Utah, Salt Lake City, UT 84112, U.S.A

and

A. R. SCHALLERT and P. SKOGERBOE
Department of Mechanical Engineering, U.S. Naval Postgraduate School, Monterey, CA 93943, U.S.A

(*Received* 18 *July* 1994 *and in final form* 27 *February* 1995)

Abstract—Heat transfer in transitional curved channel flow is investigated over a range of Dean numbers less than 300. The channel aspect ratio is 40, radius ratio is 0.979 and the ratio of boundary layer thickness to channel width is 0.011. Forced convection Nusselt numbers show the influences of Dean vortex pairs and other transitional phenomena. In particular, Nusselt numbers on the concave surface become higher than ones measured at the same streamwise location on the convex surface just after the start of curvature. Important Nusselt number increases also occur due to the twisting secondary instability as the Dean number increases from 150 to 200.

INTRODUCTION

Flows in curved channels and ducts are of interest both because of the opportunities they provide for fundamental investigations of transitional phenomena and because of the diversity of their practical applications. For the former, environments are offered to study centrifugal instabilities which are different from boundary layers and Taylor–Couette passages. In contrast to these weakly non-parallel open flows and parallel closed flows, channels and ducts are categorized as parallel open flows. Practical applications include a variety of technological and physical problems such as heat exchangers, internal turbine blade cooling passages, passages in biological systems and ducting in internal combustion engines, among others.

The present work is focused on curved channel heat transfer and energy transport, another important area of practical application. This topic is also of fundamental interest regarding both the effects of transition on heat transfer and the effects of heat transfer on transition. If Dean numbers [$De = Ud/v\sqrt{(d/r_i)}$] exceed critical values in a channel with large aspect ratio, transition from laminar flow proceeds first with the development of secondary flows near the concave surface. These eventually form into arrays of counter-rotating Dean vortex pairs [1–3] as the flow convects downstream. A variety of secondary instabilities follow the development of this primary instability depending on streamwise location and Dean number magnitude relative to values at the neutral stability curve. These include undulating wavy motions [4], spanwise wavenumber selection [5], splitting and merging of vortex pairs [5] and twisting wavy motions [3, 4]. Eventually, twisting inspires the initiation of local turbulence regions, which eventually increase in magnitude and spatial extent to form ultimately into a fully turbulent flow [4]. The secondary flows from these different phenomena, particularly the Dean vortex pairs, have long been speculated to have important effects on surface heat transfer. The present work was conducted to address this issue, in particular because heat transfer data to illustrate these effects must be obtained with forced convection alone *without* buoyancy influences and because such experimental data are very scarce in the archival literature.

In other studies of curved channel heat transfer, Cheng and Akiyama [6] and Mori *et al.* [7] numerically predicted steady, fully developed laminar forced convection in channels with uniform heat flux boundary conditions. Cheng and Akiyama employed aspect ratios ranging from 0.2 to 5, whereas Mori *et al.* used a square channel. Ratios of (perimeter-averaged) curved channel Nusselt number to straight channel Nusselt number at the ends of their ducts for $Pr = 0.71$ range from 1.05 to 2.3 [6] and from 2.3 to 4.1 [7]. In both investigations, temperature and velocity results showed clear evidence of secondary flows. Mori *et al.* [7] also presented measured spatially-averaged Nusselt numbers which showed agreement with analytic results for fully developed laminar and turbulent flows. Yee *et al.* [8] developed numerical

NOMENCLATURE

c_p	specific heat at constant pressure
d	channel height
De	Dean number
D_H	hydraulic diameter
g	gravitational acceleration
Gr	Grashoff number, equation (7)
h	heat transfer coefficient, equation (4)
k	thermal conductivity
l	length of half channel span
$\dot{m}$	mass flow rate
Nu	spanwise-averaged Nusselt number, equation (5)
Pr	Prandtl number
t	time-averaged local temperature
t_m	mixed-mean temperature
t_w	local wall temperature
u_θ	streamwise mean velocity
u'	fluctuating streamwise velocity
U	bulk mean velocity
V_c	bulk flow velocity induced by natural convection
x	streamwise distance from location where heating begins
X	streamwise distance from channel inlet at nozzle exit
Y	distance normal from the concave surface
Z	spanwise distance from channel spanwise centerline.

Greek symbols

β	volumetric coefficient of thermal expansion
Δt	$(t_w - t_m)$
ν	kinematic viscosity
ω_θ	streamwise time-averaged vorticity
ω_r	radial time-averaged vorticity
ω_z	spanwise time-averaged vorticity
θ	angular position in channel from start of curvature.

Superscripts

$\bar{}$	time-average.

schemes to predict steady laminar flow in constant temperature channels with aspect ratios of 0.33, 1 and 3. Perimeter-averaged Nusselt numbers at the downstream end of their curved domain ranged from 12 to 14. The study is similar to earlier studies [6, 7] because no buoyancy effects were included. It is different because the streamwise development of Nusselt numbers and secondary motions were predicted. Chilukuri and Humphrey [9] were the first to investigate the influences of buoyancy on developing heat transfer on laminar flow in a curved square channel. Steady numerical predictions conducted with buoyant forces aligned with and opposed to the main flow direction showed significantly different Nusselt numbers and secondary flows with streamwise development. Perimeter-averaged Nusselt numbers at the end of their curved duct ranged from 14 to 16. Komiyama [10] presented numerical schemes to predict fully developed Nusselt numbers and secondary flows in steady curved channel flows with no buoyancy influences. Channel aspect ratios ranged from 0.8 to 5, and constant heat flux boundary conditions were imposed. Several configurations of vortex pairs were predicted at low to moderate Dean numbers. At Dean numbers greater than 150–310, additional vortex pairs were predicted along with increased Nusselt numbers. Like the results of Cheng and Akiyama [6], Nusselt numbers relative to straight channel values increased as the aspect ratio decreased at a particular Dean number, with (curved to straight, perimeter-averaged) Nusselt number ratios ranging from 1.2 to 2.8

Even though numerical predictions of transitional phenomena in curved channels may ignore the effects of buoyancy, experiments cannot. Velocities are generally low enough to be of the same order of magnitude as buoyancy induced velocities, particularly near surfaces, and temperature differences must be large enough to obtain accurate heat transfer coefficients. In this investigation, Dean numbers ranged from 100 to 300, which corresponded to bulk mean velocities from 0.84 to 2.53 m s^{-1}, and differences between mixed mean and wall temperatures were as high as 18–20°C. Natural convection effects were thus important and existed simultaneously with forced convection.

In the present investigation, Nusselt numbers in mixed convection were measured first. Forced convection Nusselt numbers in transitional curved channel flow without the influences of natural convection were then determined from these measurements. To accomplish this task, buoyancy influences were minimized by orienting the channel so that gravity acted in the spanwise direction perpendicular to the bulk flow direction. In addition, a new procedure was applied to deduce forced convection Nusselt numbers from Nusselt numbers measured in a mixed convection environment with relatively weak buoyancy. Nusselt numbers deduced with this approach then clearly showed the influences of Dean vortex pairs and other important transitional phenomena. Such data are particularly important because only one other study known to the authors [7] presents *measured* heat transfer in a laminar or transitional channel flow, although there are a considerable number of publications which address turbulent heat transfer in channels.

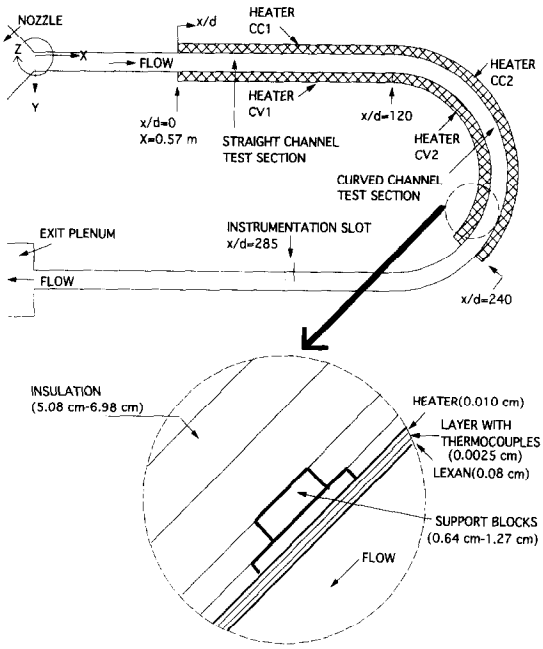

Fig. 1. Coordinate system and schematic of the curved channel used for heat transfer measurements.

EXPERIMENTAL APPARATUS

Curved channel

The rectangular cross-section curved channel shown in Fig. 1 was designed and constructed especially for this study. The interior rectangular cross-section is 1.27 (1/2) × 50.1 cm (20 in), giving an aspect ratio of 40. This large aspect ratio was chosen to minimize the influences of side walls and the Eckmann vortices which form there. In addition, adequate space was provided for repeated spanwise periodicity of vortex pairs forming across the channel span. The ratio of boundary layer thickness to convex radius of curvature δ/r_i is 0.011 in the curved section, which indicates mild curvature. Interior dimensions are dimensionally identical to those in the transparent channel employed by Ligrani and Niver [3], and Ligrani *et al.* [4, 5], so that heat transfer and flow results from the two channels can be compared. The present heat transfer channel is different from the transparent channel since it is instrumented for heat transfer measurements and because it allows longitudinal and spanwise thermal expansion of channel surfaces as they are heated. Skogerboe [11] and Schallert [12] provide additional details of the design and construction of the channel.

Prior to entering the channel, a number of devices are used to reduce spatial non-uniformities in the flow. These include a circular lip inlet, an aluminium honeycomb, three wire screens and a 20 : 1 contraction ratio nozzle. After exiting the nozzle, air first enters a straight section, 2.44 mm (96 in) in length, of which the last 1.52 m is heated, with interior dimensions of 1.27 × 50.8 cm (0.5 × 20 in). The straight section allows a hydrodynamically and thermally fully developed channel flow to develop before the flow enters the curved section which follows under most conditions studied. Flow entering the curved section is hydrodynamically fully developed for Dean numbers less than 560 [13]. The fluid then enters a 180° curved channel section with a convex surface radius of 59.69 cm (23.5 in) and a concave surface radius of 60.96 cm (24 in). The interior walls of the heated section are made of 0.08 cm thick Lexan. Upon exiting the curved section, air then enters a second straight section, also with a length of 2.44 m (96 in).

On the second straight section attached to the convex wall, a 5.08 cm (2.0 in) wide slot is present which allows insertion of a probe into the channel to measure outlet mixed mean temperatures. The slot is located approximately 57.1 cm (22.5 in) from the trailing edge of the heater on the curved convex wall, or 19.05 cm (7.5 in) downstream of the end of curvature. Two thin foam strips provide an air tight seal between the channel interior and exterior as the probe is traversed. As flow leaves the second straight portion, it passes through four screens, a honeycomb, a diffuser and finally into the first of two plenum chambers maintained at vacuum pressure. Channel air mass flow rates are determined from measurements of the pressure drop across an orifice plate with a 3.81 cm (1.5 in) hole located in piping between the two plenums.

Four etched foil heaters, manufactured by the Electrofilm Corporation, are installed to heat both the concave and convex surfaces of the channel, all at the same power dissipation rates, to produce uniform heat flux boundary conditions at the channel walls. Each heater is powered by a Superior Electric type 136B Variac. The dimensions of each heater are 38.1 × 152.4 cm (15.0 × 60.0 in), and maximum power capacity is 2 kW. In Fig. 1 CC1 and CV1 are used to designate the two heaters on the concave and convex surfaces of the straight section, respectively, and CC2 and CV2 are used to designate the heaters on the concave and convex surfaces of the curved section, respectively. To minimize heat conduction away from the test surfaces and to maximize convected heat into the channel air stream, the outsides of the channel from just upstream of the heaters CC1 and CV1 to the slot located downstream of heaters CC2 and CV2 are insulated with black foam insulation manufactured by the Halstead Company. The thickness is 5–7 cm (2.0–2.75 in).

Thermocouples were placed to provide sufficient data to determine spanwise-averaged Nusselt numbers at different streamwise locations. For this purpose, 100 copper–constantan thermocouples were placed just beneath the 0.08 cm thick Lexan channel surfaces (on sides not exposed to the airstream) to allow spatially resolved surface temperature measurements to be made. Twenty-five thermocouples were placed beneath each of the CC1, CV1, CC2 and CV2 heater surfaces in five spanwise rows of five per row. The first row of thermocouples was located 103.64 cm (40.8 in) from the inlet or 15.24 cm (6 in) from the leading edge of the first heater. Each additional row

was spaced 30.48 cm (12 in) apart in the streamwise direction. The thermocouples were placed over a spanwise length of approximately 10.16 cm (4.0 in) on each side of the centerline.

Forty more thermocouples were placed in the insulation to determine conduction heat loss. These thermocouples were placed in pairs along the channel centerline behind each row of thermocouples. This arrangement allows the temperature drop through the insulation to be measured and the conduction loss through the insulation to be determined along all segments of the test section. Two additional thermocouples were used to measure mixed mean temperature at the channel inlet and mixed mean temperature at the channel outlet.

Data acquisition system

For surface temperature measurement, voltages from the 142 thermocouples were read by Hewlett-Packard type 44422T 20 channel relay multiplexer card assemblies for T type thermocouples. These assemblies were installed in an HP3497A low-speed Data Acquisition/Control Unit and an HP3498A Extender. This system provides thermocouple compensation electronically such that voltages for type T thermocouples are given relative to 0°C. This system is connected to a Hewlett-Packard 9836A computer which processes voltages from the 142 thermocouples which are then recorded into data files along with corresponding temperatures.

EXPERIMENTAL PROCEDURES

Nusselt numbers

As the test conditions were set up, heater power levels were adjusted to provide a constant surface heat flux boundary condition along the instrumented test surfaces. The channel was heated to thermal equilibrium during which channel surfaces expanded to the sizes they assumed as measurements were made. After reaching thermal equilibrium, C-clamps were installed along the curved section to ensure that no leakage occurred from the exterior to the interior of the channel. Measurements were then made to determine local Nusselt numbers.

To do this, the power supplied to each heater was first determined from measurements of current I and voltage drop V. Convected and conducted energy flux levels were subsequently determined over each of 10 segments of the heated test section on each channel surface. Each segment was 38.1 × 30.48 cm with a row of five thermocouples along the center. Convective heat flux $\dot{q}''_{\text{conv}}$ was then determined using an equation of the form:

$$\dot{q}''_{\text{conv}} = (IV - \dot{q}_{\text{cond}})/A \tag{1}$$

where A is the surface area of each segment and $\dot{q}_{\text{cond}}$ is the conduction power loss. Using the energy balance equation given by

$$t_{\text{m}} = t_{\text{m-inlet}} + (\dot{q}''_{\text{conv}} b \Delta x)/\dot{m} C_{\text{p}} \tag{2}$$

and t_{m}, the local mixed mean temperature at any streamwise channel location was determined. Here, $t_{\text{m-inlet}}$ is the mixed mean temperature at the channel inlet, b, is the spanwise width of the heated surface and Δx is the streamwise distance from the beginning of heating to the streamwise station of interest. The corrected wall temperature t_{w} is given by

$$t_{\text{w}} = t_{\text{w-uc}} - C_{\text{r}} \dot{q}''_{\text{conv}} \tag{3}$$

where $C_{\text{r}} = 0.0034°\text{C m}^2\ \text{W}^{-1}$, as determined from experiment, and $t_{\text{w-uc}}$ is the uncorrected temperature. The last term accounts for thermal contact resistance between thermocouples and Lexan surfaces, and the temperature drop with conduction through the 0.08 cm thick Lexan surfaces. With these data, local heat transfer coefficients and local Nusselt numbers are then given by

$$h = \dot{q}''_{\text{conv}}/(t_{\text{w}} - t_{\text{m}}) \tag{4}$$

and

$$Nu = hD_{\text{H}}/k \tag{5}$$

respectively.

Exit mixed mean temperature

To calculate the local mixed mean temperature at the exit of the heated test section at each Dean number, surveys of velocity and of temperature are needed. The thermocouple probe used for this measurement was inserted through the slot described earlier and traversed over spanwise/normal planes using an automated two-dimensional traversing deice controlled by the 9836A computer. The same device was used to mount the miniature five-hole pressure probe [14, 15] used for the velocity measurements. For each traverse, 320 local temperatures or local pressures (used to determine local velocities) were recorded over a channel cross-section area of 5.08 cm (2.0 in) in the spanwise direction by 0.89 cm (0.35 in) in the radial direction in increments of 0.127 cm (0.05 in). The mixed mean temperature is then given by

$$t_{\text{m}} = \frac{1}{A_{\text{ch}} U} \int_{A_{\text{ch}}} u_0 t \, \text{d}A \tag{6}$$

where A_{ch} is the cross-sectional area of the channel. The temperature and velocity traverses cover 80% of the central portion of the channel cross-section. Regions closer to the walls have very little effect on the magnitude of t_{m} in equation (6). Additional details are given by Choi [16].

Local mean velocity

The miniature five-hole probe described by Ligrani *et al.* [14] was used to measure total pressure and the three mean velocity components locally at different locations across the channel cross-section. The tip diameter of the probe was 1.22 mm to minimize flow

blockage and maximize spatial resolution in the confined channel interior. Additional corrections to account for finite spatial resolution and streamline displacement effects were made during data reduction following Ligrani *et al.* [15].

Longitudinal velocity fluctuations

Surveys of streamwise mean velocity and longitudinal velocity fluctuations were obtained using Dantec 55P04 single hot-wire probes. Sensor diameter and length were 5 μm and 1.25 mm, respectively. Each probe was operated at an overheat ratio of 1.8 using a Dantec 55M10 constant-temperature bridge. Individual probes were calibrated in the freestream flow of a wind tunnel using procedures for low velocity measurement described by Ligrani and Bradshaw [17]. These hot-wire probes were mounted in spanwise/radial planes 120° from the start of curvature using the same automated two-dimensional traverse employed for the miniature five-hole pressure probe. Signals were conditioned with an amplifier gain of 2, a low-pass filter of 1.0 kHz, and no high-pass filter. Data were acquisitioned at 2500 Hz using a Hewlett-Packard 6944A Series 200 Multiprogrammer with a buffered 69759A analog-to-digital conversion card capable of 12-bit binary resolution. This multiprogrammer was controlled by a Hewlett-Packard Model 310 Series 9000 Computer, which also stored and processed the data. With this acquisition system, 20000 data samples were obtained at each measurement location, which amounts to a sampling interval of 8.0 s.

MIXED CONVECTION EFFECTS

The procedure to determine forced convection Nusselt numbers from Nusselt number measurements in mixed convection with weak buoyancy was described by Ligrani and Choi [18]. For a given Dean number, flow conditions and streamwise location, the procedure first requires the measurement of Nusselt numbers at different $\beta\Delta t$ where Δt is local $(t_w - t_m)$. Different $\beta\Delta t$ are produced simply by changing the power supplied to test surface heaters. This parameter was chosen because it is directly related to the magnitude of natural convection through its proportionality to the Grashoff number, which is given by an equation of the form

$$Gr = gl^3\beta\Delta t/\nu^2. \tag{7}$$

With this approach, mixed convection Nu results are measured with different magnitudes of natural convection relative to forced convection. Natural convection Nu vary significantly with $\beta\Delta t$ (and Gr) whereas forced convection Nu are independent of $\beta\Delta t$ (and Gr). Measured Nu data extrapolated to $\beta\Delta t = 0$ (and $Gr = 0$) then give forced convection Nu values with no buoyancy influences. The procedure works well for Dean numbers greater than 100. It seems to be only marginally successful at $De = 100$ since the trends of some $\beta\Delta t = 0$ data points evidence buoyancy influences.

QUALIFICATION CHECKS

The qualification tests verify procedures to determine spanwise-averaged Nusselt numbers including conduction energy balances and energy balances to calculate mixed-mean temperatures.

With mixed convection in the channel, mixed-mean temperature variations with x/d are determined from energy balances along different segments of the heated portion of the channel using equation (2), as described earlier. At $x/d = 285$, the mixed-mean temperature is also determined from direct measurement using equation (6). Plots of the surveys of mean temperature, streamwise mean velocity and velocity/temperature product used for the direct determination are given by Choi [16]. Mixed-mean temperatures from the energy balances and direct measurement at $x/d = 285$ are the same within 1.6°C for $100 < De < 300$. Such agreement verifies the correct determination of convective flux levels.

Nusselt numbers measured locally at five different spanwise locations (Z/d equals -8, -4, 0, 4 and 8) provide additional checks at 10 different x/d from 12 to 228 [12]. At high Dean numbers, excellent spanwise uniformity within 0.3 Nusselt number units indicates minimal spanwise conduction losses. At lower Dean numbers less than 50–75, small spanwise variations with Z/d evidence natural convection influences.

Additional qualification checks are provided by results in Fig. 2. This figure shows forced convection ($\beta\Delta t = 0$ and $Gr = 0$) Nusselt numbers as dependent upon x/d for Dean numbers of 100, 200 and 300. The first checks from this figure are provided by Nu data in the straight portion of the channel at x/d from 0 to 120. The match of values from the two heated surfaces at each streamwise location indicates that temperature measurements and energy balances are self-consistent. Additional verification of procedures and techniques is provided by trends of data for $x/d < 120$ which decrease with streamwise distance consistent with thermal entry length behavior.

Figure 2 also clearly illustrates spanwise-averaged Nusselt numbers which approach the expected value of 8.24 as thermal boundary layers in the straight portion of the channel merge and become fully developed at x/d from 84 to 120. $Nu = 8.24$ is expected from a simple derivation for fully developed laminar forced convection between two infinite parallel plates with constant heat flux boundary conditions. Different deviations from the expected value at different De are believed to be due to slightly different levels of thermal boundary layer development at the end of the straight portion of the channel. Finite span effects, residual buoyancy effects and/or slight data scatter may also play a role. However, in spite of any deviations due to these effects, results in Fig. 2 for

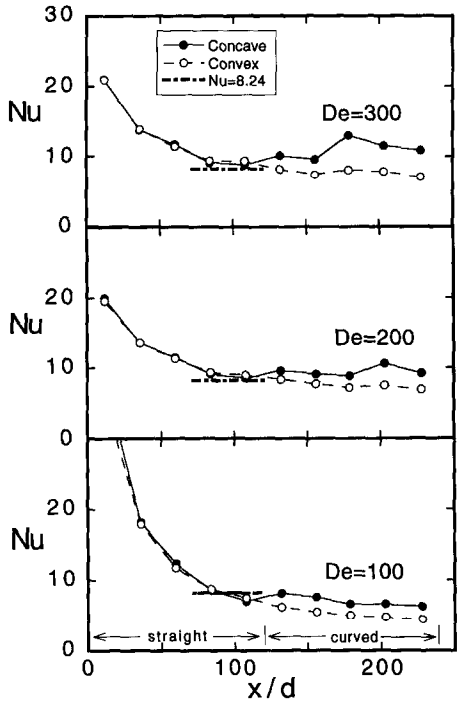

Fig. 2. Forced convection Nusselt numbers (for $\beta\Delta t = 0$) and $Gr = 0$ as dependent upon x/d for Dean numbers of 100, 200 and 300.

$x/d < 120$ provide strong evidence of the validity of the experimental procedures employed.

EXPERIMENTAL RESULTS—DEAN VORTEX DEVELOPMENT AND SURFACE HEAT TRANSFER

Figure 2 includes results from concave and convex surfaces so that differences due to curvature are apparent at x/d from 120 to 240. As mentioned in the previous section, Nusselt numbers from the two surfaces are the same over most of the straight portion of the channel. Any small Nu differences which are observed there are not considered to be significant. At the start of curvature at x/d from 120 to about 135, Nusselt numbers on the convex surface are sometimes slightly higher than those on the concave surface in some data sets, an occurrence believed to result from the mean temperature gradient in the flow immediately adjacent to the convex surface being slightly higher than the gradient at the same x/d next to the concave surface.

Further downstream, concave surface Nusselt numbers significantly exceed those measured on the convex surface. This occurs as the influences of concave curvature impose themselves on the flow. The initial increases which occur as x/d exceeds 120 – 135 are due to secondary flows which result as tiny Görtler-like vortices start to form near the concave surface of the channel. Local increases of the normal gradients of streamwise velocity and mean temperature near the concave wall probably also may play a role, especially for $De = 100$. As the Görtler-like vortices are convected downstream, they grow in spatial extent and are clearly evidenced by smoke layers near the concave surface which become spatially periodic across the channel span [3, 5]. The unsteadiness of these layers is entirely consistent with the initial development of Görtler vortices in boundary layers on concave walls, where spanwise wavelength selection mechanisms and vortex growth are very receptive to small departures from ideal flow conditions and to disturbances in the oncoming stream [5, 19]. This wavenumber selection unsteadiness along with the centrifugally induced secondary flows augment thermal transport over that produced by laminar streamwise advection alone. As a result, unsteadiness and secondary flows both play important roles in increasing concave surface heat transfer coefficients relative to those from the convex surface just after the imposition of curvature.

Such flow phenomena are further illustrated by the flow visualization photographs presented in Fig. 3. These data were obtained at $De = 122$ in a transparent curved channel [3–5] with the same internal dimensions as the channel employed for heat transfer measurements. The views presented show typical flow visualization patterns of flow cross-sections at different streamwise stations. Each covers one channel height in the Y direction and about 2.5 channel heights in the Z direction. The concave surface is at the bottom of each photograph, the convex surface is at the top, and flow is moving away from the observer. Observation locations range over θ from 65 to 145°, which correspond to x/d from 174 to 240.

As θ increases from 65 to 85°, the first three photographs in Fig. 3 show smoke layers with spatial periodicity across the channel span which increases in amplitude and definition. Such behavior is caused by the developing secondary flows in the array of partially formed vortex pairs located near the concave surface. The smoke enters the curved portion of the channel as a uniform layer about one-half channel height in extent next to the convex surface. As a result, events associated with secondary flows emanating from near the convex surface are smoke rich (bright), whereas those from near the concave surface are relatively free of smoke (dark).

As θ increases from 85 to 95°, the smoke patterns in Fig. 3 show a dramatic change as they form into clearly defined mushroom-shaped patterns. Different portions of such patterns, with their occasional unsteadiness, are closely associated with different secondary flows. The dark mushroom 'stems' with bright regions on each side are associated with upwash regions which emanate from the concave surface between the two vortices in each pair. The mushroom 'petals' correspond to vortex core regions. Bright regions between each mushroom pattern represent downwash regions (with respect to the concave surface) between vortex pairs [3]. Nu results for $De = 100$ in Fig. 2 do not show any significant change at positions corresponding to the $\theta = 85°$ and $\theta = 95°$ flow

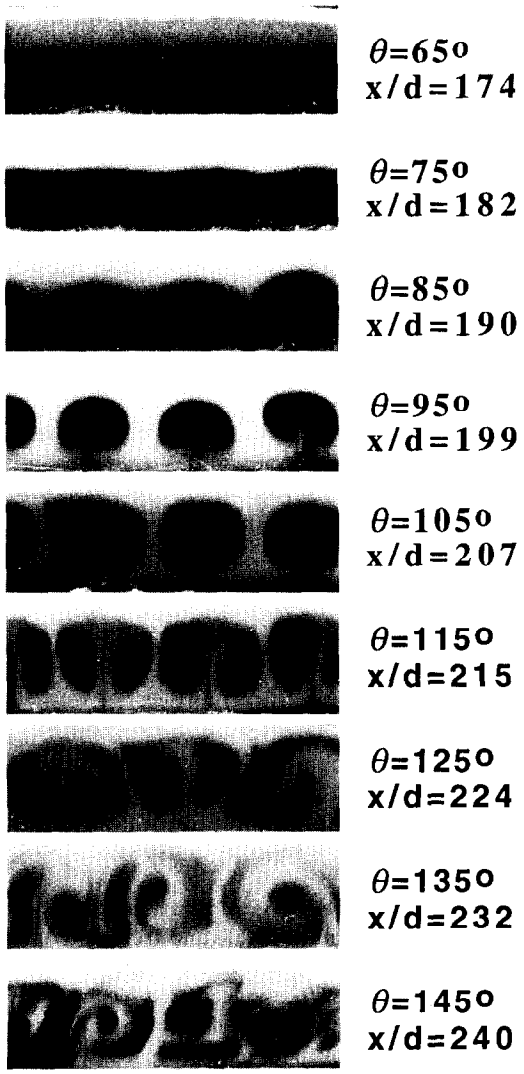

Fig. 3. Photographs of flow visualized using smoke at channel cross-sections located at different streamwise locations for $De = 122$.

visualization photographs (x/d from 190 to 199). Thus, the dramatic flow visualization pattern changes do not represent a significant change in vortex secondary flows or unsteadiness, only increased vortex development with streamwise distance. Unsteadiness and spatial variations of secondary flows continue to be higher near the concave surface, and concave Nu continue to be higher than convex values. Another factor affecting flow visualization patterns is the fact that they probably lag slightly behind the secondary flow development in vortex pairs.

As the vortex pairs continue to convect downstream, flow visualization patterns in Fig. 3 for $\theta = 105°$ and $\theta = 115°$ show patterns which increase in radial extent to occupy the full channel height. Subramanian *et al.* [20] described spanwise periodic variations of local Nusselt numbers measured in a similar type of curved channel with vortex pairs at the same De and θ. Local Nu are closely correlated with variations of the three mean velocity components across the span of the channel near the concave surface, and hence also with these flow visualization patterns. Local concave surface Nu are augmented beneath vortex pair downwash regions and diminished beneath upwash regions producing periodicity repeated over approximately each d of spanwise distance.

Time-averaged vorticity distributions which illustrate these spatial variations are shown in Fig. 4 for $\theta = 120°$ and $De = 100$. These data are determined from measurements of the three mean velocity components made using the miniature five-hole pressure probe [14, 15] in the transparent curved channel mentioned earlier [3–5]. In each plot, bulk flow direction is then into the plane of the page, $Y/d = 0$ corresponding to the concave surface and $Y/d = 1$ corresponding to the convex surface.

Radial vorticity distributions in Fig. 4(a) and streamwise vorticity distributions in Fig. 4(b) both show alternating regions of positive and negative vorticity across the channel span. An individual vortex pair is indicated by a region of positive vorticity (dashed contour lines) immediately adjacent to a region of negative vorticity (solid contour lines). Three complete pairs are evidenced in the figures; because these data were obtained at a different spanwise portion of the channel than where flow visualizations were observed, direct comparison between the two is precluded. Upwash regions corresponding to locally reduced Nu on the concave surface are positioned between the two vortices in each pair where fluid with low streamwise momentum fluid is convected away from the concave surface by secondary flows. In Fig. 4(a) and (b), central portions of upwash regions are located at Z/d of about 5.1, 6.0 and 7.1 where gradients of radial vorticity and streamwise vorticity are quite large and abrupt changes in the signs of these vorticity components occur as Z/d is changed at constant Y/d. Upwash regions are evident in spanwise vorticity distributions in Fig. 4(c) where values are large and positive. Downwash regions corresponding to locally increased concave surface Nu are positioned between vortex pairs at Z/d of 4.5, 5.5, 6.6 and 7.6. These are responsible for convection of fluid with high streamwise momentum from near the channel center to regions near the concave wall. As a result, gradients of streamwise velocity are increased locally near the concave wall [21]. Spanwise extents of upwash regions are smaller than the downwash regions as a result of higher pressure fluid existing on the downwash sides of individual vortices and lower pressure fluid existing on the upwash sides of individual vortices [20].

Some distortion of the mushroom patterns is apparent in Fig. 3 at $\theta = 115°$ which is associated with vortex pair unsteadiness, especially in the spanwise direction. These motions and distortions are more apparent at $\theta = 125°$ and are often associated with either undulating wavy motions [4] and/or spanwise wavenumber

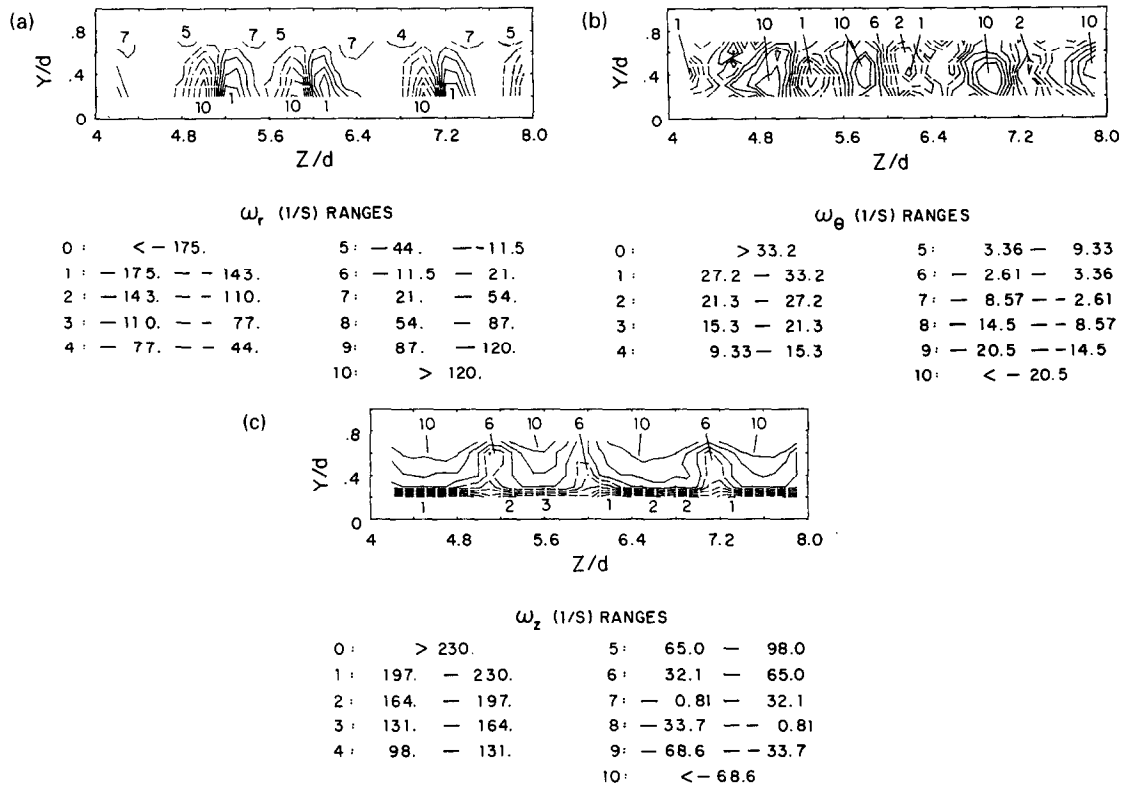

Fig. 4. Time-averaged distributions of: (a) radial vorticity; (b) streamwise vorticity; and (c) spanwise vorticity for $De = 122$, $\theta = 120°$ and $x/d = 219$.

selection resulting from splitting and merging of vortex pairs [5]. Undulations are observed for θ at least 95° at Dean numbers ranging from 40 to 125 [3, 4]. Splitting and merging are apparent in visualizations at Dean numbers from 75 to 220 [3, 5]. Comparing visualizations at $\theta = 105°$ to $\theta = 125°$ in Fig. 3 with $De = 100$ data in Fig. 2 again reveals no significant Nu changes as x/d increases from 199 to 224. Concave Nu are higher than convex Nu as before, a trend also reported by Cheng and Akiyama [6] and Yee *et al.* [8] over a wide range of θ, but in channels with significantly smaller aspect ratios.

As θ increases from 125° to 135° and 145°, smoke patterns in Fig. 3 are increasingly convoluted and distorted. Higher levels of radial and spanwise unsteadiness are present from intense undulations, frequent splitting and merging, and possibly less organized motions. $De = 100$ heat transfer data in Fig. 2 do not cover these locations, and so the effects of these combined phenomena on Nu are subject to speculation.

The Nusselt number results in Fig. 2 for $De = 200$ and $De = 300$ show some similarities to the $De = 100$ data, but also important differences. All three data sets show higher Nusselt numbers on the concave surface compared with the convex surface just after curvature is imposed on the flow as x/d becomes just greater than 120–130. At larger x/d, concave surface Nusselt numbers for the two higher Dean numbers show another important increase as the channel flow is advected. This occurs as x/d increases from 180 to 204 for a Dean number of 200 and from 156 to 180 for a Dean number of 300. For $De = 200$ (and probably also for $De = 300$), the increased Nu are associated with significantly increased flow unsteadiness.

Flow visualization photographs spaced at 1/60 s intervals in Fig. 5(a) for $x/d = 186$ ($\theta = 80°$) and $De = 200$ illustrate flow events just prior to this high unsteadiness. They show considerable distortion from radial and spanwise motions. However, in spite of this motion, clearly defined mushroom-shaped smoke patterns are still apparent indicating vortices which continue to be coherent. Such is not the case when the channel flow is convected to $x/d = 219$ ($\theta = 120°$). Smoke patterns photographed at this experimental conditions in Fig. 5(b) are located downstream of the Nusselt number increase and are so disrupted by unsteadiness that very little coherence is evident. As such, distortions of smoke are far greater than observed at $x/d = 186$ at $De = 200$ [Fig. 5(a)] and at x/d from 232 to 240 at $De = 100$ (Fig. 3).

The unsteadiness in Fig. 5(b) at $De = 200$ is most probably occurring just downstream of the twisting secondary instability [3, 4]. Twisting wavy motions manifest themselves at principal frequencies from 55 to 90 Hz as rocking vortex pair motions when observed in cross-section. Spectra measured at Dean numbers from 129 to 200 indicate that twisting energy levels may be as much as two orders of magnitude greater than levels in surrounding fluid motions near

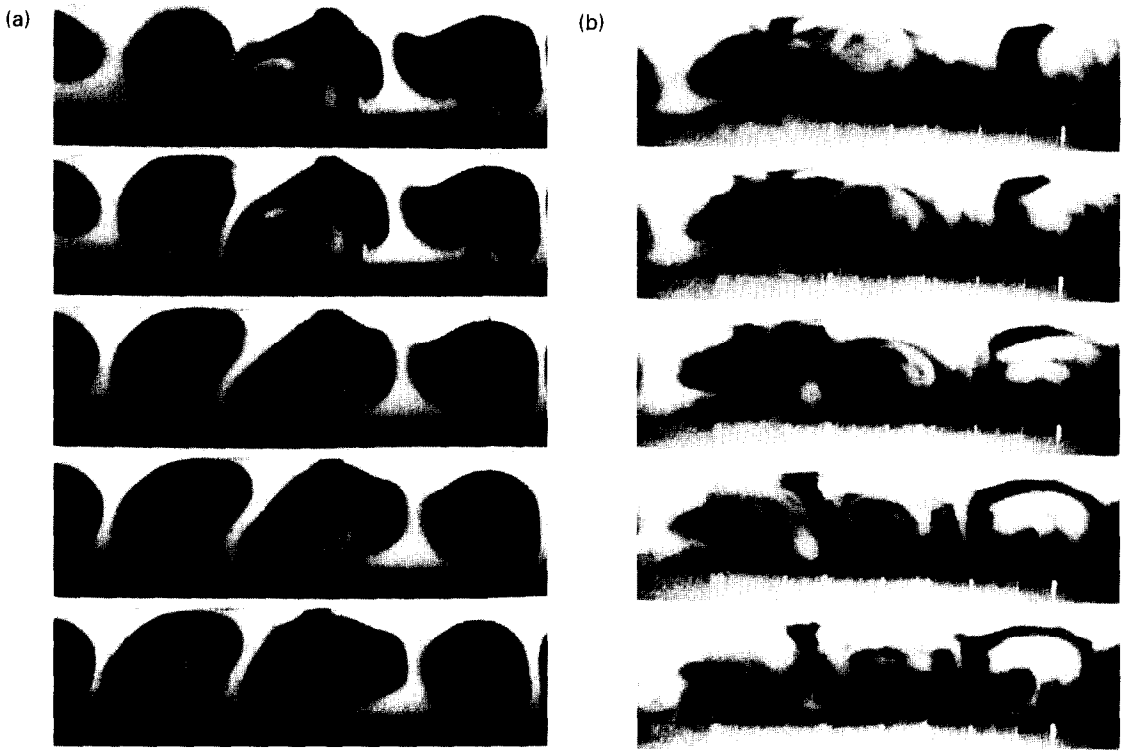

Fig. 5. Photographs of flow visualized over channel cross-sections using smoke for: (a) $De = 200$, $\theta = 80°$ and $x/d = 186$; and (b) for $De = 200$, $\theta = 120°$ and $x/d = 219$. Photographs in sequence are separated by 1/60 s intervals with time increasing as one moves down the page.

the principal frequency [4]. According to Ligrani and Niver [3] and Matsson and Alfredsson [22], at a Dean number of 200, twisting is most likely to be present at θ from 95 to 115°. The unsteadiness evident in Fig. 5(b) ($\theta = 120°$) and the Nu increase with x/d from 180 to 204 (θ from 72 to 101°) at $De = 200$ in Fig. 2 are thus both consequences of unsteadiness initiated by twisting. Twisting is the only event currently understood to be powerful enough to induce these phenomena, and both events occur at the same streamwise locations as twisting or just downstream of twisting.

EXPERIMENTAL RESULTS—EFFECTS OF DEAN NUMBER ON SURFACE HEAT TRANSFER

Concave surface measurements are presented in Fig. 6(a) and convex surface measurements are presented in Fig. 6(b) to illustrate the effects of Dean number on Nusselt number distributions. In both cases, several $De = 100$ data points at smaller x/d are left off of the plots because they are believed to be affected by natural convection effects.

Referring to the curved portion of the channel, the most interesting changes occur at x/d greater than 156. There, Nusselt numbers from both channel surfaces increase significantly as the Dean number increases from 150 to 200. This is due to two effects. First, these channel locations and experimental conditions coincide with the presence of twisting vortex motions, as mentioned earlier. Second, the thermal boundary

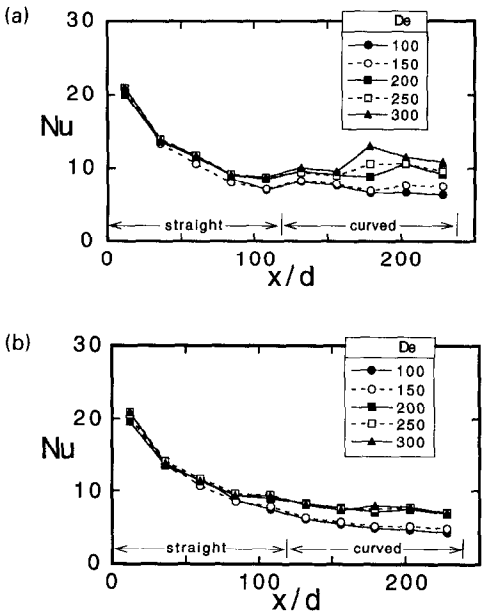

Fig. 6. Forced convection Nusselt numbers (for $\beta\Delta t = 0$ and $Gr = 0$) as dependent upon x/d and Dean number for: (a) a concave surface; and (b) a convex surface.

layers at the exit of the straight portion of the channel may be at different stages of development as De changes from 150 to 200, which results in different Nu magnitudes and different initial conditions at the inlet to

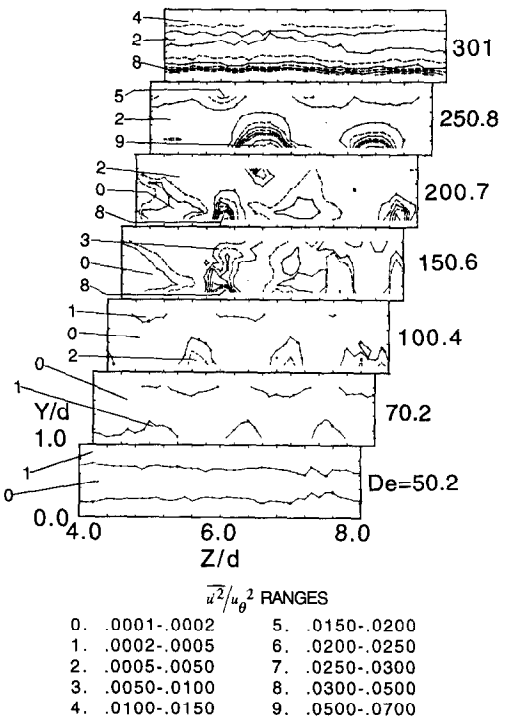

Fig. 7. Time-averaged surveys of the square of the longitudinal fluctuating velocity normalized by local mean velocity at different Dean numbers for $\theta = 120°$ and $x/d = 219$.

the curved portion of the channel. The more influential of these at $x/d > 156$ is twisting, which is probably also partially responsible for the Nu increases which occur at $x/d > 200$ as Dean number increases from 100 to 150. In spite of these Nusselt number increases from twisting, values are still generally lower than those from curved channels with smaller aspect ratios [6–10]. As De increases above 200, Nusselt numbers from the concave surface at $x/d > 150$ continue to increase with De in Fig. 6(a), whereas convex surface Nusselt numbers in Fig. 6(b) show almost no variation with De.

Results presented in Fig. 7 provide some additional rationale for these differences. Here, distributions of $\overline{u'^2}/u_0^2$, the time-averaged square of the longitudinal fluctuating velocity normalized by local mean velocity, are presented over a channel cross-section at $\theta = 120°$ for a range of De. At $De = 50.2$, fluctuating velocity distributions are spanwise uniform with very low magnitudes and similar values near each channel surface. As the Dean number increases to 70.2, small local increases near the concave surface are evident due to the unsteadiness accompanying the initiations of vortex pairs. At $De = 100.4$, maximum $\overline{u'^2}/u_0^2$ increases further over very small portions of the measurement area at locations corresponding to vortex upwash regions. Here, longitudinal fluctuations are due to undulations, splitting and merging, and other vortex pair unsteadiness.

As the Dean number increases to 150.6, twisting begins to become locally important and $\overline{u'^2}/u_0^2$ increases are probably mostly due to the twisting motion itself within and near vortex upwash regions, and partially a result of fluid, which in some cases is agitated by nearby twisting. As De increases at a particular x/d, or as x/d increases at a particular De, twisting first appears in upwash regions near the concave surface. With additional development, twisting produces intense large scale oscillations about upwash regions which correspond to variations in time and space of the streamwise velocity and secondary flows near the concave wall [4]. Twisting and these unsteady events resulting from it are thus most responsible for the increases in local and spanwise-averaged Nusselt numbers which occur as the Dean number increases from 150 to 200. Between these two flow conditions, maximum $\overline{u'^2}/u_0^2$ from twisting first occur away from the channel walls at Y/d from 0.2 to 0.4, and then throughout upwash regions near the concave surface [4].

As the Dean number increases further to 250.8, twisting motions are not seen in spectra [4]; however, the small pockets of longitudinal fluctuating velocity, such as the ones in Fig. 7 near the concave surface, show dramatic increases in magnitude. At this stage, they are probably partially associated with longitudinal Reynolds normal stresses. These eventually increase even further in spatial extent and magnitude, until the $\overline{u'^2}/u_0^2$ distribution is approximately spanwise uniform for $De > 260$. Such smearing of the local variations probably results from unsteadiness in flow induced by upstream twisting and significant local spanwise motions of vortex pairs. The higher magnitudes of unsteadiness near the concave surface and their dependence on De account both for the higher concave Nu relative to the convex surface, and the concave Nu changes which occur with De. The spanwise uniform distribution at $De = 301$ in Fig. 7 exemplifies this with significantly higher $\overline{u'^2}/u_0^2$ values near the concave surface compared with the convex surface.

SUMMARY AND CONCLUSIONS

Forced convection Nusselt numbers from a curved channel with aspect ratio of 40 are always higher on the concave surface relative to the convex surface in the curved portion of the channel, except possibly just after the imposition of curvature. The phenomena most responsible for the higher concave Nusselt numbers are vortex pair secondary flows and unsteadiness. Both of these result from the initial development of Dean vortex pairs near the concave surface in the form of tiny Görtler-like vortices whose spanwise wavelength selection mechanisms and growth rates are very receptive to small departures from ideal flow conditions and to disturbances in the oncoming stream. After the formation of Dean vortex pairs, spanwise-averaged Nusselt numbers show little variation with streamwise development in spite of the presence of spanwise wavenumber selection, splitting,

merging, undulating wavy motions, as well as less organized vortex pair motions. These invariant spanwise-averaged Nu with x/d coincide with augmented local Nusselt numbers beneath vortex pair downwash regions and diminished local heat transfer coefficients beneath upwash regions.

As the curved channel flow convects further downstream, significant increases of Nusselt numbers on the concave and convex surfaces occur with x/d as x/d becomes greater than 158 and as De becomes greater than 150. After this initial increase, concave surface Nusselt numbers at a particular streamwise station continue to increase with Dean number by important amounts, whereas convex Nu values do not. Both of these observations occur at or after the same experimental conditions as the twisting wavy secondary instability. Thus, twisting and the unsteady events caused by it and associated with it are believed to play important roles in augmenting Nusselt numbers at the downstream end of the curved portion of the channel, especially on the concave surface. In particular, twisting is associated with significantly higher longitudinal velocity fluctuations near the concave surface compared to regions near the convex surface at Dean numbers from 150 to 200. Similar trends continue to be observed at Dean numbers as high as 300.

Acknowledgements—The work presented was sponsored by the Propulsion Directorate, U.S. Army Aviation Research and Technology Activity-AVSCOM through NASA-Defense Purchase Request C-30030-P. The authors also acknowledge interesting conversations on this research with Professor M. D. Kelleher.

REFERENCES

1. W. R. Dean, Fluid motion in a curved channel, *Proc. R. Soc. Lond., Series A* **121,** 402–420 (1928).
2. D. B. Brewster, P. Grosberg and A. H. Nissan, The stability of viscous flow between horizontal concentric cylinders, *Proc. R. Soc. Lond., Series A* **251,** 76–91 (1959).
3. P. M. Ligrani and R. D. Niver, Flow visualization of Dean vortices in a curved channel with 40 to 1 aspect ratio, *Physics Fluids* **31,** 3605–3617 (1988).
4. P. M. Ligrani, W. H. Finlay, W. A. Fields, S. J. Fuqua and C. S. Subramanian, Features of wavy vortices in a curved channel from experimental and numerical studies, *Physics Fluids A* **4,** 695–709 (1992).
5. P. M. Ligrani, J. E. Longest, M. R. Kendall and W. A. Fields, Splitting, merging and spanwise wavenumber selection of Dean vortex pairs, *Exp. Fluids* **18,** 41–58 (1994).
6. K. C. Cheng and M. Akiyama, Laminar forced convection heat transfer in curved rectangular channels, *Int. J. Heat Mass Transfer* **13,** 471–490 (1970).
7. Y. Mori, Y. Uchida and T. Ukon, Forced convective heat transfer in a curved channel with a square cross section, *Int. J. Heat Mass Transfer* **14,** 1787–1805 (1971).
8. G. Yee, R. Chilukuri and J. A. C. Humphrey, Developing flow and heat transfer in strongly curved ducts of rectangular cross section, *ASME J. Heat Transfer* **102,** 285–291 (1980).
9. R. Chilukuri and J. A. C. Humphrey, Numerical computation of buoyancy induced recirculation in curved square duct laminar flow, *Int. J. Heat Mass Transfer* **24,** 305–314 (1981).
10. Y. Komiyama, Laminar forced convection heat transfer in curved channels of rectangular cross-section, *Trans. Japan Soc. Mech. Engrs B* **50,** 424–434 (1984).
11. P. E. Skogerboe, Local and spatially averaged heat transfer distributions in a curved channel with 40 to 1 aspect ratio for Dean numbers from 50 to 200, M.S. Thesis, U.S. Naval Postgraduate School, Monterey, CA (1990).
12. A. R. Schallert, A study of Nusselt number distributions in a curved channel, M.S. Thesis, U.S. Naval Postgraduate School, Monterey, CA (1992).
13. F. P. Incropera and D. P. De Witt, *Introduction to Heat Transfer* (2nd Edn). John Wiley, New York (1990).
14. P. M. Ligrani, B. A. Singer and L. R. Baun, Miniature five-hole pressure probe for measurement of mean velocity components in low speed flows, *J. Phys. E-Scient. Instrum.* **22,** 868–876 (1989).
15. P. M. Ligrani, B. A. Singer and L. R. Baun, Spatial resolution and downwash velocity corrections for multiple-hole pressure probes in complex flows, *Exp. Fluids* **7,** 424–426 (1989).
16. S. Choi, A study of surface heat transfer in a curved channel at low Dean numbers, M.S. Thesis, University of Utah, Salt Lake City, UT (1994).
17. P. M. Ligrani and P. Bradshaw, Subminiature hot-wire sensors: development and use, *J. Phys. E-Scient. Instrum.* **20,** 323–332 (1987).
18. P. M. Ligrani and S. Choi, Mixed convection in straight and curved channels with buoyancy orthogonal to the forced flow, submitted for publication.
19. H. Bippes, Experimental study of the laminar–turbulent transition of a concave wall in a parallel flow, NACA Technical Memorandum 75243, 1–69 (1978).
20. C. S. Subramanian, P. M. Ligrani and M. F. Tuzzolo, Surface heat transfer and flow properties of vortex arrays induced artificially and from centrifugal instabilities, *Int. J. Heat Fluid Flow* **13,** 210–223 (1992).
21. P. D. McCormack, H. Welker and M. D. Kelleher, Taylor–Goertler vortices and their effect on heat transfer, *ASME J. Heat Transfer* **92,** 101–112 (1970).
22. O. J. Matsson and P. H. Alfredsson, Curvature- and rotation-induced instabilities in channel flow, *J. Fluid Mech.* **210,** 537–563 (1990).